OBSERVING MODE ATTITUDE CONTROLLER FOR THE LUNAR RECONNAISSANCE ORBITER

Philip C. Calhoun and Joseph C. Garrick
NASA Goddard Space Flight Center, Code 595, Greenbelt, MD, 20771

ABSTRACT

The Lunar Reconnaissance Orbiter (LRO) mission is the first of a series of lunar robotic spacecraft scheduled for launch in Fall 2008. LRO will spend at least one year in a low altitude polar orbit around the Moon, collecting lunar environment science and mapping data to enable future human exploration. The LRO employs a 3-axis stabilized attitude control system (ACS) whose primary control mode, the "Observing mode", provides Lunar Nadir, off-Nadir, and Inertial fine pointing for the science data collection and instrument calibration. The controller combines the capability of fine pointing with that of on-demand large angle full-sky attitude reorientation into a single ACS mode, providing simplicity of spacecraft operation as well as maximum flexibility for science data collection. A conventional suite of ACS components is employed in this mode to meet the pointing and control objectives.

This paper describes the design and analysis of the primary LRO fine pointing and attitude re-orientation controller function, known as the "Observing mode" of the ACS subsystem. The control design utilizes quaternion feedback, augmented with a unique algorithm that ensures accurate Nadir tracking during large angle yaw maneuvers in the presence of high system momentum and/or maneuver rates. Results of system stability analysis and Monte Carlo simulations demonstrate that the observing mode controller can meet fine pointing and maneuver performance requirements.

INTRODUCTION

The Lunar Reconnaissance Orbiter (LRO) mission is the first of a series of lunar robotic spacecraft scheduled for launch in Fall 2008. LRO will spend at least one year in a low altitude polar orbit (mean altitude approx. 50km) around the Moon, collecting lunar environment science and mapping data to enable future human exploration. The objective is to provide key science data necessary to facilitate human return to the Moon as well as identification of excellent opportunities for future science missions. LRO's instrument suite will provide the high resolution imaging data with sub-meter accuracy, highly accurate lunar cartographic maps, and mineralogy mapping, amongst other science data of interest.

The LRO employs a 3-axis stabilized attitude control system (ACS) whose primary control mode, the "Observing mode", provides Lunar Nadir, off-Nadir, and Inertial fine pointing for the science data collection and instrument calibration operations. The Observing mode controller is required to maintain fine pointing during the operation of a large fully-articulated solar array that maintains solar incidence normal to the array surface. This mode is also required to maneuver to off-Nadir attitudes, ensuring opportunities for capturing important science data. In addition, large angle maneuvers are required for the purposes of performing delta-V and station keeping operations, solar array pointing, instrument calibration, and Nadir attitude acquisition from Sun pointing or other inertial attitudes. A conventional suite of ACS components is employed in this mode to meet the pointing and control objectives. Actuation is provided by a set of four reaction wheels developed in-house at NASA Goddard Space Flight Center (GSFC), with momentum unloading provided by a reaction control system (RCS) also developed in-house. The attitude determination function utilizes two Galileo Avionica Autonomous Star Trackers (A-STR), and a single Honeywell Miniature Inertial Measurement Unit (MIMU).

The Observing mode controller is required to provide fine Nadir pointing with an absolute accuracy of 45 arc-sec (3 sigma) and knowledge of 30 arc-sec (3 sigma) measured relative to the prime AST reference. An on-board ephemeris interpolator generates Nadir attitude targets used for nominal science data collection. Attitude determination is performed by a six-state Multiplicative Extended Kalman Filter (MEKF) with three attitude states

Page intentionally left blank

Table 2. Star Tracker Performance Parameters

Parameter	Requirement (Attitude rate < 0.3 deg/sec)	
(All errors are shown for output quaternion)		
	Bias + Systematic (arc-sec, 3 σ)	Random (arc-sec, 3 σ)
Transverse Error	11	36
Roll about Boresight Error	30	120

Reaction Wheels

The LRO spacecraft has four reaction wheels onboard to provide control torque during the Observing control modes. The wheels are sized to provide adequate momentum storage to meet the momentum dumping frequency requirement of two weeks. The reaction wheels are manufactured at NASA/GSFC by the Component Hardware Systems Branch, in the Mission Engineering and Systems Analysis (MESA) Division. The four wheels are aligned in pyramid fashion with the apex of the pyramid centered on the spacecraft's +X body axis. This alignment was determined as the best for the expected momentum accumulation. A level of redundancy exists in case of a single wheel failure. However, in this condition the ACS can not meet the two week momentum unloading interval. Table 3 provides a list of the reaction wheel performance requirements relevant to this study. The momentum capacity of 80 N-m-sec is the requirement for low bus voltage of 24 Volts. The 60 N-m-sec level is the maximum level expected before momentum unloading during typical science operations. The torque noise requirement is a PSD specification on the allowable broadband noise below 1 Hz. Reaction wheel imbalance requirements are not given in this paper since their jitter effects, along with all other jitter sources, are not considered part of the ACS pointing accuracy budget.

Table 3. Reaction Wheel Performance

Parameter	Requirement
Momentum Capacity	80 N-m-sec 60 N-m-sec (nominal limit)
Maximum Torque Cmd	0.16 N-m
Torque Noise (root PSD)	3e-4 N-m/Hz$^{1/2}$
Coulomb Friction	+/- 0.004 N-m
Torque Cmd. Quantization	15 bit (D/A)

OBSERVING CONTROLLER

The Observing controller is a quaternion-feedback, proportional-integral-derivative (PID) controller used to produce reaction wheel torque commands. A mathematical description of the body control torque, $\vec{T}_c$, is provided by Equation 1. In this equation, the first three terms are referred to as the PID torque, denoted as $\vec{T}_{PID}$, and the last term is referred to as the gyroscopic compensation term. This form of the controller is similar to the quaternion feedback control law presented in Ref. 3. The body control torque is comprised PID terms involving rate error, $\vec{\omega}_e$, attitude error, $\vec{a}_e$, and integral of attitude error, using the feedback gains $k_r, k_p,$ and k_i. The following parameters are also included in the definition of the body control torque; $I_B^{B^*}$, the Inertia matrix of the spacecraft about its mass center B^*, $\vec{h}_W$, RW angular momentum, and, $\vec{\omega}_B$, the estimated spacecraft body rate.

$$\vec{T}_c = I_B^{B^*}\left(k_r\vec{\omega}_e + k_p \text{proplim}[\vec{a}_e] + k_i\int\vec{a}_e\right) + \vec{\omega}_B \times (I_B^{B^*}\vec{\omega}_B + \vec{h}_W) \qquad (1)$$

Page intentionally left blank

The wheel momentum redistribution torque is computed using the Mini-Max wheel momentum redistribution law [4], given in Eq. 5, where $k_{h_W redist}$ is the wheel momentum redistribution gain given in Table 4. This law tends to minimize the maximum of the individual wheel momentum, thus tending to drive pairs of wheels at the same speed in the same direction. The limit in Eq. 5 is set to 0.02 N-m in the simulation studies performed for LRO.

$$\vec{T}_{h_W redist} = \lim\left[-k_{h_W redist}\,\tfrac{1}{2}\left(\max(h_W) + \min(h_W)\right)\right] \tag{5}$$

Table 4. Observing Controller Parameters

Parameter	Symbol	Value
Rate gain	k_r	0.4 sec^{-1}
Position gain	k_p	0.057 sec^{-2}
Integral gain	k_i	0.0023 sec^{-3}
Wheel Mom. Redist. gain	$k_{h_W redist}$	0.01 N-m
Structural filter (3^{rd} order)		Passband ripple = 0.1 dB Stopband Attenuation = 35 dB Roll-off frequency = 0.35 Hz

Alternate RW Torque Command

The LRO baseline algorithm for determining the wheel torque commands is given by Eq. 4. The proportional limiting is performed on the sum of the filtered control torque, drag compensation, and momentum redistribution torques. This method has a potential defect; it does not necessarily preserve the direction of the filtered PID torque when RW commands exceed the proportional limits. An alternative method for implementing the wheel torque commands is motivated from the fact that it is important to preserve the filtered PID torque direction to produce the desired motion control during large angle slews, as discussed in the previous controller section. This is accomplished by applying proportional limiting separately to the filtered PID torques. It is also important to preserve the other torques, particularly the gyroscopic compensation torques, which dominate the RW commands when the system momentum is high. Of course there is a trade-off between limiting the RW compensation torques versus the filtered PID torques when torque saturations occur.

The solution is to first map the gyroscopic compensation torques to wheel space, and then compute a limited RW compensation torque expressed in wheel space, $\vec{T}_{RWcomp\lim}{}^{W}$, as shown in Eq. 6. This limit ensures that there will be some residual wheel torque available for the filtered PID control torque, so that the system can be stabilized and the maneuver completed successfully. In practice this residual torque can be quite small for the controller to still maintain the slew performance.

$$\vec{T}_{RWcomp\lim}{}^{W} = \lim\left[A_{WB}\left[\vec{\omega}_B \times (I_B^{B*}\vec{\omega}_B + \vec{h}_W)\right] + \vec{T}_{Wdrag} + \vec{T}_{h_W redist}\right] \tag{6}$$

Now, compute the upper bound on the filtered PID torque allowed for each wheel, $T_{PID\,filt}{}^{W}\big|_{Ubnd}$. This is accomplished by subtracting the limited RW compensation torques from the total upper bound on the wheel commands, $\vec{T}_W\big|_{Ubnd}$. The numerical values computed for each wheel's upper bound are dependent upon the signs of the filtered PID torques expressed in wheel space, $\vec{T}_{PID\,filt}{}^{W}$, as shown in Eq. 8. This produces a larger value for the allowable filtered PID torques when the RW compensation torques are in opposite directions.

$$\vec{T}_{PID\,filt}{}^{W} = -A_{WB}\,\vec{T}_{PID\,filt} \tag{7}$$

Page intentionally left blank

all modeled with 0.1 % damping with the exception of the slosh mode which is modeled with 1% damping. Slosh mode damping is set to one tenth of the expected value to ensure conservative results since this mode tends to interact with the SA modes and reduce damping for the low frequency system modes.

The stability analysis is conducted by breaking the control loop at three locations; angle, rate, and torque feedback. Margins were evaluated for nominal model parameters with selected parameter variations. These included +/- 20% variations for Inertias, flexible mode gains, slosh mass, and slosh stiffness, and +/- 25% variations for flexible mode frequencies. Worst case margins over all FEM configurations for the nominal control parameters with parameter variations are shown in Table 5. Breaking the loop at the torque feedback results in the lowest predictions for gain margin (9.5 dB) and modal suppression (12.9 dB); while breaking at angle feedback results in the lowest phase margins (39.2 deg). The lowest frequency structural modes had frequencies of approximately 1 Hz.

Results of the stability analysis demonstrated that all structural modes are gain stabilized with adequate stability margins. Some of the low frequency modes have large modal gain, which, when coupled with the rather conservative assumption of 0.1 % modal damping, made the modal suppression requirement difficult to achieve. A 3rd order elliptic filter is used for structural mode filtering in order to meet the modal suppression requirement in the presence of parameter variations.

Table 5. Summary of Linear Stability Analysis Results (lowest margins obtained are highlighted)

	Break at Torque			**Break at Angle**			**Break at Rate**		
Flex Body (Param. Variations)	**X axis**	**Y axis**	**Z axis**	**X axis**	**Y axis**	**Z axis**	**X axis**	**Y axis**	**Z axis**
Gain Margin (dB)	9.5	9.5	9.9	16.0	16.0	16.0	11.8	9.9	9.9
Phase Margin (deg)	46.7	44.6	44.2	45.2	39.2	39.2	59.1	51.3	51.1
Modal Suppression (dB)	12.9	13.7	14.6	47.2	47.4	50.2	30.3	13.9	14.8

SIMULATION STUDIES

The observing mode controller is analyzed in several simulation studies using a high fidelity Monte Carlo simulation of the closed loop dynamics to demonstrate worst case expected ACS performance. The spacecraft ephemeris is simulated for a circular orbit with nominal altitude of 50 km above the Lunar surface. The simulation includes rigid body system dynamics with time varying system inertia due to SA and HGA gimbal motion. Nominally, when the Observing controller is operational, the SA is gimbaled to track the Sun and the HGA is gimbaled to track Earth ground stations. The simulation also includes high fidelity models of the ACS flight hardware, data interfaces, and ACS algorithms, as well as environmental disturbances due to gravity gradient and solar pressure. This model, developed using Matlab's Simulink toolbox, is used by the LRO ACS analysis team to assess ACS performance and validate the ACS flight algorithms. Monte Carlo variables include all sensor and actuator error sources, initial body rates, initial RW momentum, and inertias. For each scenario described below the initial RW momentum is varied within the expected range (60 N-m-sec) during Observing mode operations, and the spacecraft inertia is varied by +/- 20% from the nominal values.

The simulation includes error source and disturbance models for the A-STR, IRU, and RW each at their respective requirement levels for assessment of the worst case pointing performance. The AST model includes random noise and bias/systematic errors at the required LRO performance specifications, given in Table 2. AST performance degradation due to ST occultation from the Sun, Earth, and Moon entering within the A-STR FOV is also modeled in the simulation. The IRU noise parameters, including scale factor variations, are modeled at the LRO requirements levels given in Table 1. In addition, slowly varying misalignments due to thermal effects between the IRU and A-STR mounting were modeled with a magnitude of 100 arc-sec (3σ). Disturbance source models for the RW include wheel friction, torque noise, and torque command quantization at the LRO requirements levels given in Table 3. A nominal RW drag model is also included in the model.

Results of two simulation scenarios are shown in this section to demonstrate the Observing mode performance in two critical operational modes. A Nadir pointing scenario is shown to demonstrate the controller performance

Page intentionally left blank

Delta-V mode to begin the second burn. If more time is required to set up for the second burn the slew rate could be set higher by setting the appropriate attitude error limit. But, within the operating range of wheel momentum the wheel torques would likely exceed their limits as the slew rate increases above 0.1 deg/sec. In this situation wheel momentum unloading would be need to be performed prior to the first burn.

Results for 50 Monte Carlo simulation cases of this scenario are shown below in Figures 3 and 4. Initial rate damping and attitude stabilization is completed within 5 min after mode transition in all cases. The yaw maneuver is initiated at 10 min after controller mode transition and is completed in approximately 30 min in all cases. A steady yaw slew rate (0.1 deg/sec), set by the attitude error limit is achieved in all cases. As shown in Figures 3 and 4, the yaw slew is properly coordinated relative to the instantaneous Nadir frame. This results in a pure yaw motion with variable pitch / roll rate as the spacecraft maneuvers from +X velocity vector to the -X velocity vector Nadir attitudes. The off-Nadir roll and pitch attitude excursions are maintained at less than 1 deg during the slew as shown in Figure 3. Relatively large torques, present during the slew, primarily due to counteracting the gyroscopic effects of the RW momentum, nearly reached their limits. This indicates that the RW momentum should be dumped prior to the slew to avoid the potential for RW momentum saturation.

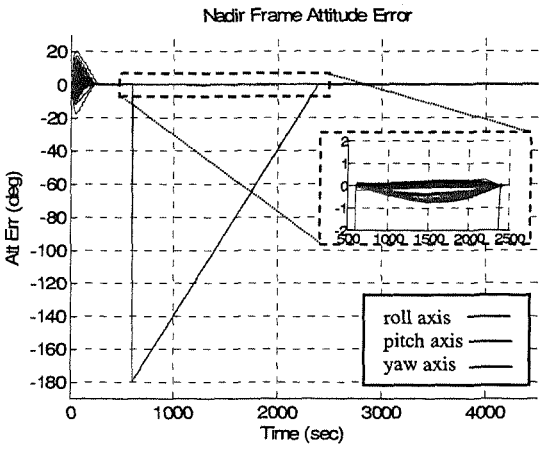

Figure 3, Yaw Slew Scenario, Attitude Error

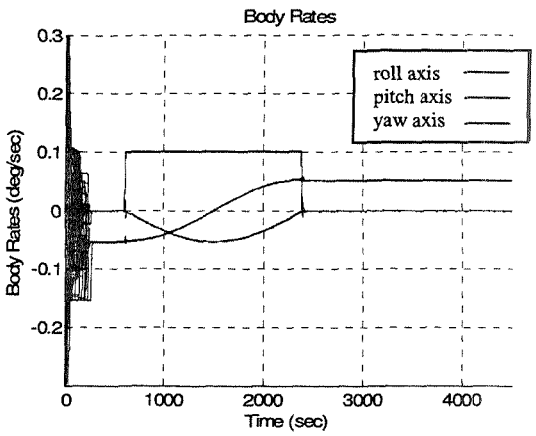

Figure 4, Yaw Slew Scenario, Body Rates

CONCLUSIONS

This paper documents the design of the LRO Observing mode controller, which combines fine pointing capability for science data collection operations with full-sky large-angle slew capability into a single ACS control mode. The results from linear system stability analysis and two simulation studies, using the LRO high fidelity simulation, demonstrate the LRO fine pointing and large angle slew performance. The results show robust performance in the presence of parameter variations and marginal ACS hardware performance. Fine pointing and stability requirements are achieved with margin. Nadir target attitude excursions during large angle yaw slews are limited to less than 1 deg, ensuring direct sunlight avoidance for the Nadir pointing instrument suite during occasional 180 deg yaw slews.

An alternate method is developed for computing the RW torque commands, which uses proportional limiting of the filtered PID torque commands to preserve the PID torque vector direction. This method was compared against the baseline approach using the LRO high fidelity simulation. No significant performance improvement has been observed in studies performed to date. For this reason, and because of flight software implementation issues associated with the alternate method, the baseline approach was chosen as the method to carry forward to software development. However, it is thought that the alternative method holds promise to provide improved performance, possibly in scenarios not studied thus far. Future work should perform more extensive studies to determine whether or not this method is useful in improving control performance and stability during large angle slews that induce RW torque saturation.